ACS APPLIED ENERGY MATERIALS

www.acsaem.org

Letter

All Platinum-Group-Metal-Free Alkaline Exchange Membrane Water Electrolyzers Using Direct Hydrothermal Catalyst Deposition on Raney Ni Substrate

Malte Klingenhof, Sören Selve, Christian M. Günther, Johannes Schmidt, Fatemeh Razmjooei,* Peter Strasser,* and Syed-Asif Ansar

Cite This: *ACS Appl. Energy Mater.* 2024, 7, 6856−6861

Read Online

ACCESS | Metrics & More | Article Recommendations | Supporting Information

ABSTRACT: Green hydrogen produced via water electrolysis powered by renewable energy sources promises the decarbonization of large sectors of the economy. Despite alkaline environments that enable use of non-noble, abundant materials, state-of-the-art anion exchange membrane water electrolyzers (AEMWEs) uses noble-metal-based catalysts. Developing non-noble-metal-based anodes would enhance the competitiveness of AEMWEs. Herein, an anode fabricated by hydrothermal deposition of binder-free NiFe-LDH onto Raney Ni (RNi) substrates is described. The introduced platinum-group-metal-free AEMWEs display high performance of 1 A cm^{-2} at 1.9 V cell voltage. Physicochemical characterization highlights the successful combination of NiFe-LDH with RNi applying a scalable synthesis offering feasibility to fabricate active and durable electrodes for AEMWEs.

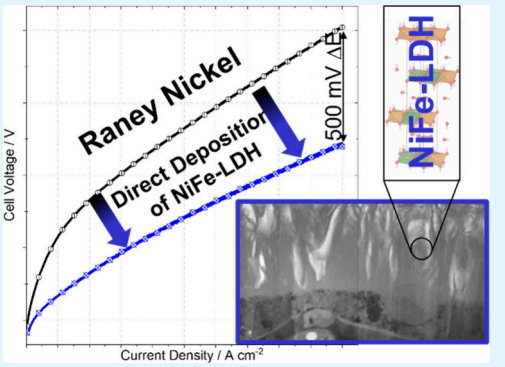

KEYWORDS: *AEMWE, non-noble, NiFe-LDH, PFAS-free, interlayer optimization*

Green hydrogen will be playing a key role in decarbonizing power production, industrial processes, heat generation, as well as mobility.[1] Cost reduction of the production of green hydrogen is critical to trigger its wider use: today, 96% of all global hydrogen is still produced by steam cracking.[1] Water electrolysis providing H_2 and O_2 via electrochemical splitting of water ($H_2O \rightarrow H_2 + 1/2\ O_2$) is a zero CO_2-emission alternative if renewable energy sources are used. Low temperature water electrolysis technologies, such as alkaline electrolysis (AEL), polymer electrolyte membrane water electrolyzers (PEMWEs), and anion exchange MWEs (AEMWEs), are in different stages of R&D and commercialization.[2] AEL is the most mature technology with industrial applications.[2] Nevertheless, low operation current densities accompanied by large stack sizes and slow start−stop operation limit integration with renewables. PEMWEs offer high current densities and hydrogen production rates, small stack sizes, and fast start-up and shut-down operation. Despite the key advantages of PEMWEs over AEL, global deployment of PEMWE technology depends on the availability and circular economy of necessary critical raw materials. Rare platinum group metal (PGM) based electrodes combined with noble-metal-coated cell components and fluorinated polymers necessary to sustain the harsh applied acidic conditions are expensive. In particular, iridium with its volatile cost accompanied by low annual production of 8.5 t tied to the supply of platinum places a bottleneck for realization of required market goals.[3,4] AEMWEs combine the advantages of both technologies. High current densities and small stack sizes offer opportunities for integration with renewables. Furthermore, high pH environments are compatible with abundant and low-cost transition metal (oxyhydr)oxide catalysts and noncritical cell components. Nevertheless, AEMWEs are in the early stages of development. State-of-the-art AEMWE technology still relies on highly alkaline feeds and PGM powder electrocatalysts.[5] Recent state-of-the-art AEMWE hydrogen production rates are 1.7 A cm^{-2} at 1.8 V cell voltage with 24 wt % KOH solution (above 5 M KOH) at 80 °C.[6]

AEMWE electrocatalysts are largely applied as thin powder films on porous transport layers (catalyst coated substrate, CCS) or membranes (catalyst coated membrane, CCM). Coating techniques require ionomer binders stabilizing the powder catalyst on the substrate of choice and providing ion-conduction between the membrane and catalytically active centers. Surface blocking, introduction of nonconductive polymers, delamination and oxidation of binder polymers, and catalyst blocking accompanied by time-consuming

Received: June 28, 2024
Revised: July 26, 2024
Accepted: July 26, 2024
Published: August 5, 2024

https://doi.org/10.1021/acsaem.4c01647
ACS Appl. Energy Mater. 2024, 7, 6856−6861

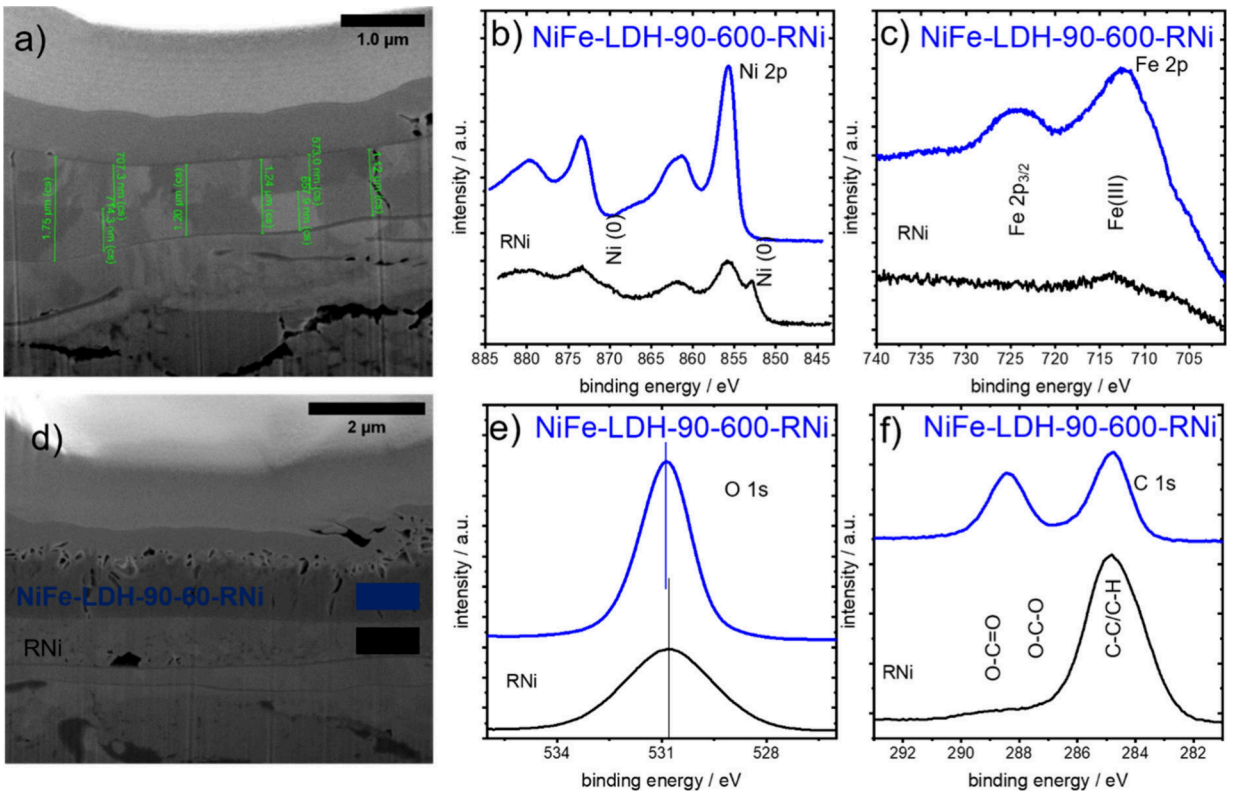

Figure 1. Morphological and electronic structure/chemical state investigations of pristine RNi substrates and hydrothermally grown NiFe-LDH-90−600-RNi composite electrodes, using FIB-SEM cross-sectional images and X-ray Photoemission. (a) FIB-SEM cross section of the RNi substrate; the RNi portion is indicated in green. (d) FIB-SEM cross-section of NiFe-LDH-90−600-RNi. (b, c, e, and f) XPS spectra in Ni 2p, Fe 2p, O 1s, and C 1s range. The black line corresponds to RNi substrate, while the blue line corresponds to NiFe-LDH-90−600-RNi.

catalyst-ink developments are significant hurdles for performance and practical application.[7,8]

Binder-free direct catalyst coating techniques overcome the limitations related to powder catalysts. However, these coating techniques are still poorly explored and, to date, have not been shown to yield electrode performance comparable to conventional powder-based catalyst layers or demand highly optimized,[9] complicated preparation techniques limiting broad application.[10] High performance catalyst coatings require the effective and easily scalable deposition of highly active catalysts onto high surface area contact layers, providing high catalyst utilization. This study addresses this unmet need reporting a direct AEMWE electrode deposition design with higher performance in AEMWE single cells than NiFe-LDH in nickel foam (NF), which places the standard material for direct catalyst deposition in the literature.[11,12] Our cell design also excludes any "hidden" PGM-coatings of porous transport layer components. We demonstrate that the cell performance is made possible by a synergistic effect between Raney-Ni (RNi) electrode substrates,[13] onto which NiFe-LDH layers were grown directly layer-by-layer. We characterized the morphology, structure, and chemical state of the NiFe-LDH@RNi composite electrodes using focused-ion beam scanning electron microscopy (FIB-SEM) as well as selected area electron diffraction (SAED) on a FIB-prepared lamella. We demonstrate that powder-free deposition results in catalyst layers that are structurally and chemically identical with conventional NiFe-LDH powder/binder-type coatings.

SYNTHESIS AND CHARACTERIZATION OF NiFe-LDH AT NF

Metal precursors, solvent, and the anode substrates were introduced in a 30 mL autoclave followed by autogenous pressure hydrothermal synthesis (detailed synthesis conditions for different sets of anodes are depicted and described in Table 1 and Figure S1). Synthesis conditions were optimized with NF (Table 1) and applied to RNi. Under hydrothermal conditions, nanostructured NiFe films grew in situ on the high surface area RNi substrate. FIB cross sections of blank RNi and NiFe-LDH-90−600-RNi (Figure 1a, d) highlight the successful synthetic deposition of NiFe layers on RNi substrates. Figures 1a, d and S2 show cross sections measured with SEM and TEM of RNi before and after hydrothermal growth of NiFe overlayer. The NiFe-LDH surface appears as a tight, homogeneously bonded overlayer with a uniform interfacial contact to the RNi substrate. Inspection of the RNi substrate thickness uncovers a thinning down to 1.085 ± 0.131 μm from initially 1.260 ± 0.170 μm after NiFe-LDH deposition. The thickness of the NiFe-LDH layer is 1.446 ± 0.307 μm. This may suggest that the NiFe-LDH layer growth penetrated roughly 200 nm into the RNi substrate, favoring a uniform RNi/NiFe-LDH interphase with good adhesion and excellent electrical conductivity.

The FIB-SEM cross sections supported by X-ray photoelectron spectroscopy (XPS) studies reveal significant changes in the elemental compositions and chemical states of near-surface species during the synthesis. Figure 1b, c, e, and f highlight photoemission core level spectra in the Ni 2p, Fe 2p, O 1s, and C 1s range of NiFe-LDH-90−600-RNi and the

https://doi.org/10.1021/acsaem.4c01647
ACS Appl. Energy Mater. 2024, 7, 6856−6861

pristine RNi substrate. Ni 2p core level shifts (Figure 1b) clearly show changes in the chemical states of Ni near the surface. RNi substrates (black line) showed metallic Ni^0 as well as oxidized Ni species. By contrast, NiFe-LDH-90−600-RNi (blue line) showed oxidic Ni species only, while the metallic Ni contribution disappeared. Comparison of Fe 2p core level peaks of NiFe-LDH-90−600-RNi and pristine RNi substrates (Figure 1 c) reveals distinct FeOx signals expected for the LDH overlayer. The RNi substrate shows only weak signals originating from the Ni LMM Auger process. Overall, the electronic structure and chemical states of NiFe-LDH-90−600-RNi reflected in its Ni 2p and Fe 2p spectra evidence the hydroxide character of the NiFe top layer. This is further supported by changes in the core levels of O 1s and C 1s (Figures 1e and S3). As expected, the photoemission O 1s and C 1s spectra (Figures 1e, f and S3) evidenced atmospheric carbon residues, with NiFe-LDH-90−600-RNi also displaying distinct O−C−O and O−C═O signals arising from interlayer CO_3^{2-} anions, present in the LDH interlayer. This is further strong evidence for the successful direct hydrothermal growth of NiFe-LDH onto RNi substrates.[14,15] Our surface sensitive analysis confirms the characteristic elemental composition and electronic structure of a NiFe-LDH overlayer grown on the RNi substrate, forming a uniform interphase offering good adhesion between substrate and overlayer.

STEM-EDS mappings of NiFe-LDH-90−600-RNi revealing the elemental composition and the interaction between RNi and the NiFe top layer are depicted in Figures S4 and S5 and are discussed in the Supporting Information (SI). While combined SEM/XPS analyses of NiFe oxide layers have been reported before,[16] direct structural evidence of the characteristic crystallography of overgrown NiFe-LDH top layers have remained elusive. Using selected area electron diffraction (SAED) on FIB-lamella, we succeeded in recording characteristic electron diffraction directly of the hydrothermally deposited NiFe-LDH overlayers (Figure 2). X-ray diffraction patterns of powder NiFe-LDH (Figure 2a) are in agreement with SAED measurements of NiFe-LDH-90−600-RNi (Figure 2b and c). Figure 2b plots the SAED-derived scattered electron intensity versus lattice parameter $d_{(hkl)}$ for the NiFe-LDH-90−600-RNi sample. The presence of the characteristic (003) and (006) reflection evidence the formation of the layered ion-incorporated NiFe-LDH phase on the RNi substrate. Comparisons with SAED measurements of the NiFe-LDH powder are depicted and discussed in the SI (Figure S6). TEM-Micrographs of the FIB-lamella which are used for the SAED study (Figure 2d−f) highlight the interaction between NiFe-LDH lamellas and the RNi substrate.

Furthermore, the interphase between the RNi substrate and deposited NiFe-LDH thin film is displayed in detail in Figures 2e and S4 confirming that NiFe-LDH directly grew into and onto the RNi substrate.

ELECTRODE DESIGN AND PERFORMANCE OF "ALL PGM-FREE" AEM WATER ELECTROLYZER

Optimized NiFe-LDH catalyst layer deposition conditions for highly active anode designs, reaction times at 160 °C, and rpm during the hydrothermal LDH layer growth on NF were systematically varied. Table 1 summarizes the NiFe-LDH@NF-X-Y (X: reactions time at 160 °C; Y: rpm during synthesis) results. Since the oxygen evolution reaction (OER) performance of Ni-based anodes is strongly influenced by the Ni/Fe ratio,[17] anodes were prepared varying the Ni/Fe ratio

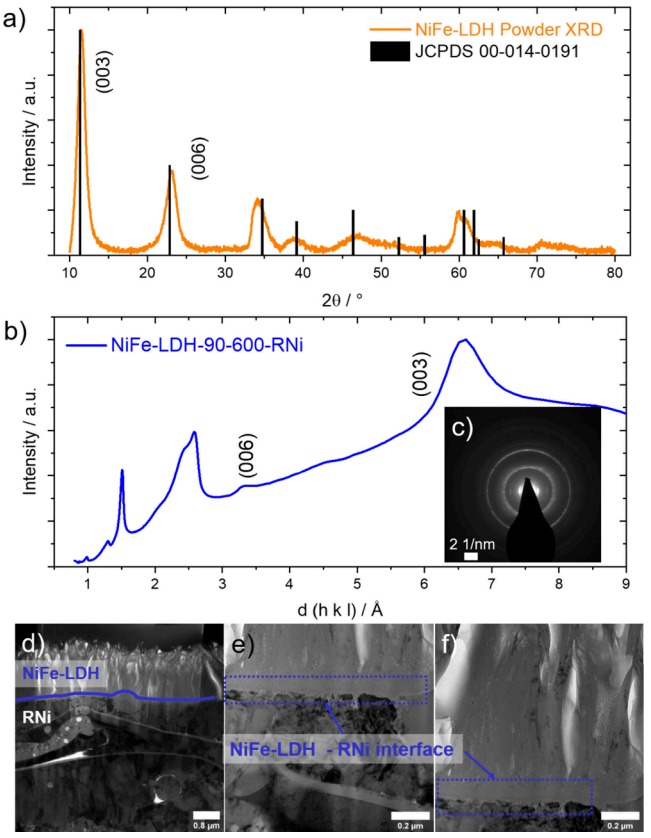

Figure 2. Powder X-ray diffraction pattern (XRD) and TEM investigations of the hydrothermally prepared NiFe-LDH-90−600-RNi electrode. (a) XRD pattern of NiFe-LDH powder (orange line) including XRD reference for powder samples (JCPS 00−014−0191, black columns). (b) Line profile of electron diffraction pattern of NiFe-LDH-90−600-RNi (blue line) derived by radial integration along central line as depicted in (c) SAED of NiFe-LDH-90−600-RNi. (d−f) TEM images of the sample area applied to SAED measurements.

influencing the resulting electrochemical activity toward OER. Measured performances are depicted in the SI (Figure S7). Since RNi places an additional Ni source in the synthesis, adjusting the Ni/Fe ratio by varying the Ni/Fe ratio of the synthesis mixture turns out to be more complicated with only a minor impact on the electrocatalysis of the anodes. The resulting anodes were implemented into AEM single cell water electrolyzers, and their performance was screened and compared. The individual CCS anodes were assembled into AEMWE cells using Mo incorporated RNi cathodes, treated with Fumasep FAA-3-PK-130 (membrane) sandwiched between the two CCSs. Fumasep FAA-3-PK-130 was utilized because a comparison with AEMION membranes revealed advantageous behavior of the electrodes used with Fumasep FAA-3-PK-130 (Figure S8). The cells were operated with 1 M KOH feed at 60 °C (Table 1 and Figure 3a and b).

Figure 3a presents the experimental polarization curves of "all PGM-free" AEMWE cells with four different kinds of NiFe-LDH@NF anodes from Table 1, operated at 60 °C in 1 M KOH. The cell incorporating the NiFe-LDH@NF-90−600 anode featured the lowest AEMWE cell voltage of 1.82 V at 0.5 A cm^{-2}, outperforming NiFe-LDH@NF-60−600 (1.89 V), NiFe-LDH@NF-90−300 (1.95 V), and NiFe-LDH@NF-60−300 (1.96 V) and revealing the 90−600 synthesis conditions as favorable. Thus, these specific synthesis conditions were

https://doi.org/10.1021/acsaem.4c01647
ACS Appl. Energy Mater. 2024, 7, 6856−6861

Table 1. AEMWE cell performance screenings at 1.8 V cell voltage and 60°C of "all PGM-free" AEMWE employing directly hydrothermally grown NiFe LDH overlayers on NF or RNi substrate. Sample names include synthesis conditions. See SI for synthesis details

Anode	Current Density A cm^{-2} in 1 M KOH
RNi substrate	0.16
NiFe-LDH@NF-60−300	0.27
NiFe-LDH@NF-90−300	0.28
NiFe-LDH@NF-60−600	0.34
NiFe-LDH@NF-90−600	0.45
NiFe-LDH-90−600-RNi	0.7

applied to the hydrothermal catalyst coating of the RNi substrates. Figure 3b compared the uncorrected polarization curves of AEMWE cells incorporating pristine, uncoated RNi anodes (black), the best performing coated NF anode from Figure 3a (NiFe-LDH@NF-90−600, violet), and the composite anode comprising both material systems under optimized synthesis conditions (NiFe-LDH-90−600-RNi, blue). The "all PGM-free" system with NiFe-LDH-90−600-RNi displayed a cell voltage of 1.73 V at 0.5 A cm^{-2}, outperforming the NF-based references. Here, the performance difference between NiFe-LDH@NF-90−600 and NiFe-LDH-90−600-RNi is highly interesting, since NiFe-LDH@NF-90−600 is the most active anode in three-electrode measurements (Figure S7). The AEMWE cell performance is made possible by the synergistic effect between catalytically active NiFe-LDH overlayers and RNi anode providing excellent catalyst utilization, improved especially compared to well-known NiFe-LDH-NF combinations.

All tested AEMWE cells operated at current densities up to 2 A cm^{-2} (Figure 3b) where the NiFe-LDH-90−600-RNi anode continued to display superior energy efficiency at a low cell voltage of 2.2 V over NiFe-LDH@NF-90−600 (2.34 V) and pristine RNi (2.71 V). To put the kinetic performance of the present "all PGM-free" AEMWE cell in perspective to state-of-art reports on PGM-free AEMWE, Figure 3c compares and contrasts the experimental current densities of today's state-of-art "all PGM-free" (blue) and PGM-containing (orange and red) AEMWE designs under comparable conditions applying Fumion-based membranes. The present

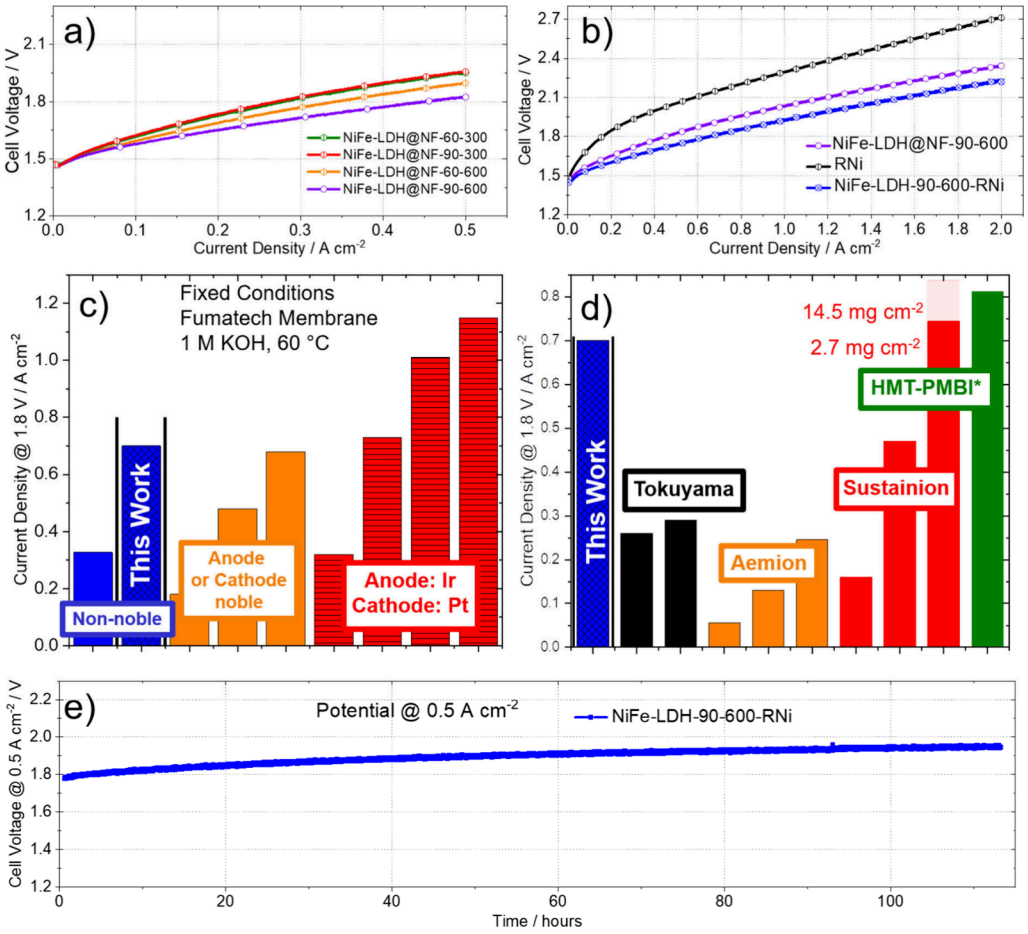

Figure 3. Electrochemical characterization of the AEMWE electrolyzer cells in 1 M KOH at 60 °C. (a) Polarization curves of AEMWE cells with different synthesis conditions applied to NF based anodes (NiFe-LDH@NF-60−300 (red), NiFe-LDH@NF-90−300 (olive), NiFe-LDH@NF-60−600 (orange), and NiFe-LDH@NF-90−600 (violet)). (b) Comparison between NiFe-LDH@NF-90−600 rpm (violet), bare RNi (black), and NiFe-LDH-90−600-RNi (blue) as anode. (c) Comparison of different catalyst materials applying Fumion based membranes and (d) literature-known values of commercially available membranes (Tokuyama, Aemion and Sustainion) applying non-noble catalyst materials as anode and cathode, both (c) and (d) at 1.8 V applying comparable operating conditions (T, KOH feed).[19−25,27−29] (e) 0.5 A cm^{-2} current hold of NiFe-LDH-90−600-RNi as anode over 110 h. Mo incorporated RNi and Fumasep FAA-3-PK-130 are used as cathodes and anion exchange membranes in all the operated cells.

https://doi.org/10.1021/acsaem.4c01647
ACS Appl. Energy Mater. 2024, 7, 6856−6861

NiFe-LDH-90−600-RNi anode design in the all PGM-free AEMWE sharply outperforms previous PGM-free and even PGM-containing system designs (Figure 3c).[18−23]

To demonstrate the performance characteristics of the presented cell design and draw attention to the difficulties in comparison, Figure 3d presents AEMWE cell current densities at 1.8 V cell voltage of state-of-art PGM-free electrodes combined with different types of commercial alkaline exchange membranes under identical operating conditions.[24−28] Tokuyama[28,29] and Aemion[24,26,28] based membranes trail our present cell design, which is matched by only one of several previously reported Sustainion-based and one self-made AEMWE cell architectures.[10,27,28] Still, the reported Sustainion-based electrolyzer cell uses high amounts of catalyst material at the electrodes.[25] The literature reports an intriguing system as the cathode is composed of comparable materials, and RNi serving as the substrate for NiFe-LDH here is employed as the anode. Through optimized MEA assemblies and self-made and much thinner (only 50 μm compared to 130 μm of the FAA-3-PK-130) membranes, they achieve higher current densities at 1.8 V.[10] Besides the self-made membrane, the electrode preparation process is challenging, requiring consistent conditions and users and limiting the preparation technique.[10] Nevertheless, Figure 3b illustrates the superior performance NiFe-LDH-90−600-RNi over the RNi anode which is in a very simple system, leaving the membrane as the only performance dictating difference between the literature-known system and the herein presented system. Thus, we once more show that the membrane chemistry, membrane thickness, and MEA assembly majorly influence overall performance. We may expect further improvements upon incorporation of further catalyst material in addition to the CCS based approach or by changing the applied membrane.[10,25]

The short-term durability of the AEMWE cell with the NiFe-LDH-90−600-RNi anode was evaluated under a constant current density of 0.5 A cm^{-2} at 60 °C. AEMWE cell voltage was monitored over about 110 h (Figure 3e). The cell voltage shows a 170 mV increment over the 110 h of operation, equivalent to 1.5 mV h^{-1}. While this is a good degradation rate for PGM- and PFAS-free AEMWE cells,[30] it is a factor of 10x larger than low Ir loaded anodes but PFAS-containing membranes and PFAS-containing porous transport layers applied in PEM water electrolysis.[4] We note that the durability of AEMWE cells continues to be largely determined by the degradation rate of the alkaline exchange membrane, which is not in the scope of this contribution.

CONCLUSIONS

We have presented an "all PGM-free" AEMWE cell and electrode design with high performance and efficiency characteristics. At 1.8 V cell voltage, a current density of 0.7 A cm^{-2} was obtained. We provided evidence that this performance was made possible by an anode electrocatalyst deposition strategy, involving the direct hydrothermal deposition of catalytically OER active NiFe-LDH overlayers onto high surface area RNi substrates. The direct hydrothermal preparation of catalyst coated anode substrates eliminated time-consuming and challenging process steps of powder catalyst preparation and handling and the preparation and stabilization of ionomer inks and pastes, followed by their uniform coating. We showed that the direct hydrothermal coating yields uniform, well-adhering, electrically conductive interphases linking the NiFe-LDH overlayer with the RNi substrate bulk. Physicochemical characterization further revealed that the directly deposited NiFe-LDH layer exhibits the characteristic structural and crystallographic features of nanostructured NiFe-LDH. Synergy between NiFe-LDH with high surface area RNi substrate gives rise to the AEMWE cell performance and cell stability. We further note that the presented electrode designs can be applied to powder-based membrane electrode assemblies to further enhance electrochemical performance.

ASSOCIATED CONTENT

Supporting Information

The Supporting Information is available free of charge at https://pubs.acs.org/doi/10.1021/acsaem.4c01647.

Description of the material, electrochemical and physicochemical characterization including calculations (PDF)

AUTHOR INFORMATION

Corresponding Authors

Fatemeh Razmjooei − *Department of Chemistry/Functional Materials, Technical University Berlin, 10623 Berlin, Germany*; Email: Fatemeh.Razmjooei@dlr.de

Peter Strasser − *The Electrochemical Energy, Catalysis, and Materials Science Laboratory, Department of Chemistry, Chemical Engineering Division, Technical University Berlin, 10623 Berlin, Germany*; orcid.org/0000-0002-3884-436X; Email: pstrasser@tu-berlin.de

Authors

Malte Klingenhof − *The Electrochemical Energy, Catalysis, and Materials Science Laboratory, Department of Chemistry, Chemical Engineering Division, Technical University Berlin, 10623 Berlin, Germany*

Sören Selve − *Center for Electron Microscopy (ZELMI), Technical University Berlin, 10623 Berlin, Germany*

Christian M. Günther − *Center for Electron Microscopy (ZELMI), Technical University Berlin, 10623 Berlin, Germany*; orcid.org/0000-0002-3750-7556

Johannes Schmidt − *Department of Chemistry/Functional Materials, Technical University Berlin, 10623 Berlin, Germany*

Syed-Asif Ansar − *Institute of Engineering Thermodynamics, German Aerospace Center, 70569 Stuttgart, Germany*

Complete contact information is available at: https://pubs.acs.org/10.1021/acsaem.4c01647

Notes

The authors declare no competing financial interest.

ACKNOWLEDGMENTS

Financial support by the federal ministry for education and research (Bundesministerium für Bildung und Forschung, BMBF) under Grant Numbers 03SF0613D "AEMready", 03HY130B "AEM-Direkt", 03SF0630C "ZnH2", the Project "ANEMEL" (Project 101071111) funded by the EISMEA (European Innovation Council and SMES Executive Agency), and the Deutsche Forschungsgemeinschaft (DFG, German Research Foundation) under Germany's Excellence Strategy—EXC 2008-390540038—UniSysCat are gratefully acknowledged.

REFERENCES

(1) Kusoglu, A. The Many Colors of Hydrogen. *Electrochem. Soc. Interface* **2022**, *30*, 44.
(2) Schalenbach, M.; et al. A Perspective on Low-Temperature Water Electrolysis − Challenges in Alkaline and Acidic Technology. *Int. J. Electrochem. Sci.* **2018**, *13*, 1173−1226.
(3) Umicore. Precious Metal Prices. *Umicore*, 2023.
(4) Suermann, M.; Bensmann, B.; Hanke-Rauschenbach, R. Degradation of Proton Exchange Membrane (PEM) Water Electrolysis Cells: Looking Beyond the Cell Voltage Increase. *J. Electrochem. Soc.* **2019**, *166*, F645−F652.
(5) Du, N.; et al. Anion-Exchange Membrane Water Electrolyzers. *Chem. Rev.* **2022**, *122*, 11830−11895.
(6) Kraglund, M. R.; et al. Ion-solvating membranes as a new approach towards high rate alkaline electrolyzers. *Energy Environ. Sci.* **2019**, *12*, 3313−3318.
(7) Li, D.; et al. Highly quaternized polystyrene ionomers for high performance anion exchange membrane water electrolysers. *Nature Energy* **2020**, *5*, 378−385.
(8) Cossar, E.; Oyarce Barnett, A.; Seland, F.; Baranova, E. A. The Performance of Nickel and Nickel-Iron Catalysts Evaluated As Anodes in Anion Exchange Membrane Water Electrolysis. *Catalysts* **2019**, *9*, 814.
(9) López-Fernández, E.; et al. Chemistry and Electrocatalytic Activity of Nanostructured Nickel Electrodes for Water Electrolysis. *ACS Catal.* **2020**, *10*, 6159−6170.
(10) Wang, L.; et al. High Performance Anion Exchange Membrane Electrolysis Using Plasma-Sprayed, Non-Precious-Metal Electrodes. *ACS Applied Energy Materials* **2019**, *2*, 7903−7912.
(11) Zhao, H.; et al. Facile, Controllable, and Ultrathin NiFe-LDH In Situ Grown on a Ni Foam by Ultrasonic Self-Etching for Highly Efficient Urine Conversion. *Environ. Sci. Technol.* **2023**, *57*, 2939−2948.
(12) Klingenhof, M.; et al. Modular Design of Highly Active Unitized Reversible Fuel Cell Electrocatalysts. *ACS Energy Letters* **2021**, *6*, 177−183.
(13) Razmjooei, F.; et al. Increasing the performance of an anion-exchange membrane electrolyzer operating in pure water with a nickel-based microporous layer. *Joule* **2021**, *5*, 1776−1799.
(14) Carrasco, J. A.; Sanchis-Gual, R.; Silva, A. S.-D.; Abellán, G.; Coronado, E. Influence of the Interlayer Space on the Water Oxidation Performance in a Family of Surfactant-Intercalated NiFe-Layered Double Hydroxides. *Chem. Mater.* **2019**, *31*, 6798−6807.
(15) Hunter, B. M.; Hieringer, W.; Winkler, J. R.; Gray, H. B.; Müller, A. M. Effect of interlayer anions on [NiFe]-LDH nanosheet water oxidation activity. *Energy Environ. Sci.* **2016**, *9*, 1734−1743.
(16) Li, H.; Wang, X.; Wang, T.; Xiao, F. A facile, green and time-saving method to prepare partially crystalline NiFe layered double hydroxide nanosheets on nickel foam for superior OER catalysis. *J. Alloys Compd.* **2020**, *844*, 156224.
(17) Gorlin, M.; et al. Tracking Catalyst Redox States and Reaction Dynamics in Ni-Fe Oxyhydroxide Oxygen Evolution Reaction Electrocatalysts: The Role of Catalyst Support and Electrolyte pH. *J. Am. Chem. Soc.* **2017**, *139*, 2070−2082.
(18) Kaczur, J. J.; Yang, H.; Liu, Z.; Sajjad, S. D.; Masel, R. I. Carbon Dioxide and Water Electrolysis Using New Alkaline Stable Anion Membranes. *Front Chem.* **2018**, *6*, 263.
(19) Campagna Zignani, S. Performance and stability of a critical raw materials-free anion exchange membrane electrolysis cell. *Electrochim. Acta* **2022**, *413*, 140078.
(20) Carbone, A.; Zignani, S. C.; Gatto, I.; Trocino, S.; Aricò, A. S. Assessment of the FAA3−50 polymer electrolyte in combination with a NiMn2O4 anode catalyst for anion exchange membrane water electrolysis. *Int. J. Hydrogen Energy* **2020**, *45*, 9285−9292.
(21) Faid, A.; Oyarce Barnett, A.; Seland, F.; Sunde, S. Highly Active Nickel-Based Catalyst for Hydrogen Evolution in Anion Exchange Membrane Electrolysis. *Catalysts* **2018**, *8*, 614.
(22) Park, J. E.; et al. Graphitic carbon nitride-carbon nanofiber as oxygen catalyst in anion-exchange membrane water electrolyzer and rechargeable metal−air cells. *Applied Catalysis B: Environmental* **2018**, *237*, 140−148.
(23) Park, J. E.; et al. High-performance anion-exchange membrane water electrolysis. *Electrochim. Acta* **2019**, *295*, 99−106.
(24) Cossar, E.; Murphy, F.; Walia, J.; Weck, A.; Baranova, E. A. Role of Ionomers in Anion Exchange Membrane Water Electrolysis: Is Aemion the Answer for Nickel-Based Anodes? *ACS Applied Energy Materials* **2022**, *5*, 9938−9951.
(25) Motealleh, B.; et al. Next-generation anion exchange membrane water electrolyzers operating for commercially relevant lifetimes. *Int. J. Hydrogen Energy* **2021**, *46*, 3379−3386.
(26) Khataee, A.; Shirole, A.; Jannasch, P.; Krüger, A.; Cornell, A. Anion exchange membrane water electrolysis using Aemion membranes and nickel electrodes. *Journal of Materials Chemistry A* **2022**, *10*, 16061−16070.
(27) Liu, Z.; et al. The effect of membrane on an alkaline water electrolyzer. *Int. J. Hydrogen Energy* **2017**, *42*, 29661−29665.
(28) Pushkareva, I. V.; Pushkarev, A. S.; Grigoriev, S. A.; Modisha, P.; Bessarabov, D. G. Comparative study of anion exchange membranes for low-cost water electrolysis. *Int. J. Hydrogen Energy* **2020**, *45*, 26070−26079.
(29) Pavel, C. C.; et al. Highly efficient platinum group metal free based membrane-electrode assembly for anion exchange membrane water electrolysis. *Angew. Chem., Int. Ed. Engl.* **2014**, *53*, 1378−1381.
(30) Fortin, P. High-performance alkaline water electrolysis using Aemion anion exchange membranes. *J. Power Sources* **2020**, *451*, 227814.

https://doi.org/10.1021/acsaem.4c01647
ACS Appl. Energy Mater. 2024, 7, 6856−6861